Q. J. R. Meteorol. Soc. (2005), **131**, pp. 1783–1792 doi: 10.1256/qj.04.125

Note on the effect of horizontal gradients for nadir-viewing microwave and infrared sounders

By J. JOINER[1]* and P. POLI[2,3]

[1]*NASA Goddard Space Flight Center, Laboratory for Atmospheres, Greenbelt, USA*
[2]*Joint Center for Earth Systems Technology, University of Maryland, Baltimore County, USA*
[3]*NASA Goddard Space Flight Center, Global Modeling and Assimilation Office, Greenbelt, USA*

(Received 10 August 2004; revised 1 December 2004)

SUMMARY

Passive microwave and infrared nadir sounders such as the Advanced Microwave Sounding Unit-A (AMSU-A) and the Atmospheric InfraRed Sounder (AIRS), both flying on NASA's EOS polar-orbiting Aqua satellite, provide information about vertical temperature and humidity structure that is used in data assimilation systems for numerical weather prediction and climate applications. These instruments scan across track so that, at the satellite swath edges, the satellite zenith angles can reach ∼60°. The emission path through the atmosphere as observed by the satellite is therefore slanted with respect to the satellite footprint's zenith. Although radiative transfer codes currently in use at operational centres use the appropriate satellite zenith angle to compute brightness temperature, the input atmospheric fields are those from the vertical profile above the centre of the satellite footprint. If horizontal gradients are present in the atmospheric fields, the use of a vertical atmospheric profile may produce an error.

This note attempts to quantify the effects of horizontal gradients on AIRS and AMSU-A channels by computing brightness temperatures with accurate slanted atmospheric profiles. We use slanted temperature, water vapour, and ozone fields from data assimilation systems. We compare the calculated slanted and vertical brightness temperatures with AIRS and AMSU-A observations. We show that the effects of horizontal gradients on these sounders are generally small and below instrument noise. However, there are cases where the effects are greater than the instrument noise and may produce erroneous increments in an assimilation system. The majority of the affected channels have weighting functions that peak in the upper troposphere (water-vapour-sensitive channels) and above (temperature-sensitive channels) and are unlikely to significantly impact on tropospheric numerical weather prediction. However, the errors could be significant for other applications such as stratospheric analysis. Gradients in ozone and tropospheric temperature appear to be well captured by the analyses. In contrast, gradients in upper stratospheric and mesospheric temperature as well as upper-tropospheric humidity are less well captured. This is likely due in part to a lack of data to specify these fields accurately in the analyses. Advanced sounders, like AIRS, will help to better specify these fields in the future.

KEYWORDS: AIRS AMSU Assimilation Azimuth angle Radiances Satellite

1. INTRODUCTION

The Atmospheric Infra-Red Sounder (AIRS) and the Advanced Microwave Sounding Unit-A (AMSU-A) (Aumann *et al.* 2003) are nadir-viewing passive sounders currently flying on the National Aeronautics and Space Administration's (NASA) Earth Observing System (EOS) polar-orbiting Aqua platform. AMSU-A also flies on the National Oceanic and Atmospheric Administration (NOAA) Polar Orbiting Environmental Satellites along with the High-resolution InfraRed Sounder (HIRS). These and other similar sounders are the primary satellite instruments used in atmospheric data assimilation systems (DASs) for numerical weather prediction and the production of climate datasets.

Fast radiative transfer models are used to compute brightness temperatures from background fields in a DAS. Analysis increments are then generated based on the difference between the observed and the computed brightness temperatures. The effects of so-called limb-brightening or limb-darkening across a scan line for an instrument on a polar-orbiting satellite are accounted for in the radiative transfer model by using an appropriate satellite zenith angle. However, the input atmospheric profile is usually the vertical one above the satellite footprint centre. The correct atmospheric profile should account for the fact that the emission path through the atmosphere is slanted with respect to the footprint zenith. If horizontal gradients are present, an error may occur if the vertical atmospheric path is used.

Horizontal gradient effects are a well-known problem for limb-viewing sounders. For example, gradient effects were shown to be important for the limb-viewing Global Positioning Satellite Radio Occultation sounding technique (e.g. Poli 2004; Poli and Joiner 2004).

* Corresponding author: NASA Goddard Space Flight Center, Code 916, Greenbelt, MD, 20771, USA.
e-mail: joanna.joiner@nasa.gov

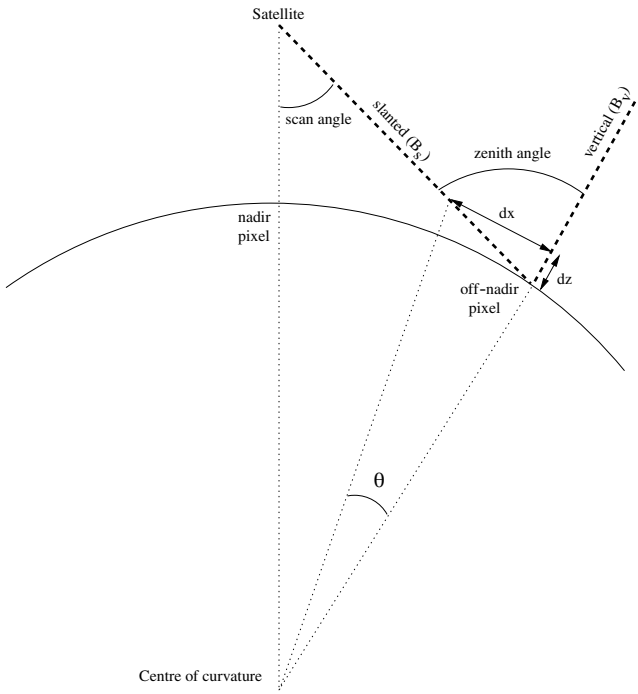

Figure 1. Schematic of AIRS footprints for nadir (left) and off-nadir (right) pixels where dx is the offset from the centre of the footprint to the actual atmospheric location of the emission path at height dz.

Over the past two decades, the amount of computing power has increased dramatically and with it the resolution of models and analysis systems. With horizontal resolutions now at the scale of tens of kilometres even for global models, gradient effects may be significant for nadir sounders. This may be especially true for advanced high-spectral-resolution sounders that have channels with peaks in weighting function at high altitudes. Here, we use analysed fields of temperature, humidity, and ozone from current data assimilation systems along with appropriate geometrical emission paths to accurately assess the effects of horizontal gradients for AIRS and AMSU-A.

Sections 2 to 5 describe the geometry, observations, background fields, and methodology, respectively, that are used to compute brightness temperatures with vertical and slanted atmospheric emission paths. In section 6 we apply the methodology to AIRS and AMSU-A channels and use observations to assess the accuracy of the gradients in the assimilated atmospheric fields. In section 7 we discuss the importance of horizontal gradients for sounders on geostationary platforms. Conclusions and suggestions for further research are given in section 8.

2. EMISSION PATH GEOMETRY

Figure 1 shows the geometry for nadir and off-nadir pixels. For the off-nadir pixel with a zenith angle α and an emission height dz, there will be an offset dx in the emission path with respect to the vertical. The usual approach to calculate a radiance from a three-dimensional field at the off-nadir pixel ignores that offset. Instead, one extracts temperature and constituent (humidity, ozone) information located at the vertical above the off-nadir pixel.

In order to calculate the radiance along the slanted line-of-sight, we need to extract the information from the analysed fields along that line. The positions of the points to consider along that line are given by applying a rotation in the plane determined by the local centre of curvature and the satellite azimuth angle. The angle of the rotation θ is shown in Fig. 1 and can be found using simple geometry.

The offset dx can be written as $\mathrm{d}x = \mathrm{d}z \cdot \tan\alpha$ and is shown in Fig. 2 for various altitudes dz. That distance dx can be compared with the horizontal resolution of the analysed fields at hand (approximately 100 km or better in the tropics and higher resolution at high latitudes for grid-point analyses and models). For heights below 10 km, we observe that the distance dx remains below 10 km even for the largest

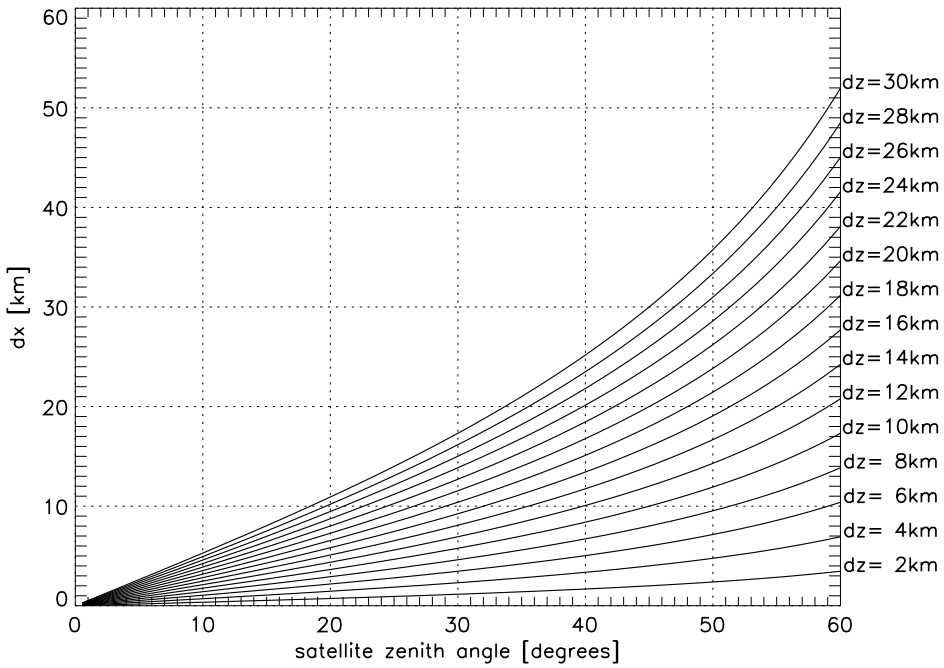

Figure 2. Horizontal offset, dx, from the centre of the footprint for off-nadir pixels versus satellite zenith angle for different emission heights, dz.

zenith angles. Consequently, we do not expect to see much difference between slanted and vertical radiative transfer calculations for channels peaking in the lower troposphere. However, for heights of 20 km or above, offsets dx larger than 10 km are obtained for all zenith angles greater than 30°. This suggests that, for upper tropospheric and stratospheric channels, using either vertical or slanted atmospheric profiles may produce significant brightness temperature differences. One could argue that the effects of larger dx offsets may be partially cancelled by smoother fields at higher altitudes. The present paper attempts to address this issue. Note that, in this paper, we neglect the effects of atmospheric refraction. These effects are negligible for the instruments and geometries used here.

3. Observations

The Aqua satellite was launched in May 2002. Here we use observations (O) from a single day (16 December 2002). We use a reduced AIRS radiance dataset (Goldberg *et al.* 2003) provided by the NOAA National Environmental Satellite Data and Information Service. This dataset contains a 281-channel subset of the 2378 available AIRS channels. We use only AMSU-A channels 3 to 14 that have a significant atmospheric contribution.

There are nine AIRS pixels within an AMSU-A footprint. For this study, we first select a single AIRS pixel within the AMSU-A footprint with the highest temperature in an 11 μm window channel. We then apply the cloud detection algorithm of Joiner *et al.* (2004) to remove cloud-contaminated channels.

4. Assimilated background fields

The background fields (B) used here come from a combination of assimilation systems. In the troposphere and lower stratosphere, temperature and humidity are from the Spectral Statistical Interpolation analysis of the National Center for Environmental Prediction (NCEP) (Derber and Wu 1998). We used the operational fields (T254L64) with a model top at 2 hPa.

In the middle stratosphere and above, temperature and humidity are from a 6-hour forecast of the NASA Global Modeling and Assimilation Office (GMAO) finite-volume data assimilation system. GMAO fields have a horizontal resolution of 1° latitude × 1.25° longitude. At the equator, this is 111 km × 140 km,

but at 60° it is 111 km × 70 km. The model top is 0.01 hPa. The general circulation model used for the GMAO DAS forecast includes the dynamical core of Lin (1997) with physics from the Community Climate Model-3 of the National Center for Atmospheric Research (Kiehl *et al.* 1996). The GMAO analysis uses the Physical-Space Statistical Analysis System (PSAS) (Cohn *et al.* 1998).

The ozone fields come from an off-line PSAS analysis with a horizontal resolution of 1° × 1.25° (Stajner *et al.* 2001). Assimilated observations were from the Solar Backscatter Ultraviolet (SBUV) radiometer.

Temperature and humidity from the NCEP and GMAO fields were combined as follows (L. Takacs, personal communication). The NCEP spectral analysis below 10 hPa was remapped to the GMAO grid-point resolution. The remapping algorithm was designed to conserve the vertically integrated column mean of the remapped variable. Above 5 hPa, only the GMAO 6-hour forecast was used. Between 5 and 10 hPa, a linear blend of the GMAO first guess with the remapped NCEP analysis was used. This combination was designed to provide accurate fields in both the troposphere and upper stratosphere to mesosphere.

5. Observed minus background ($O - B$) calculations

We use the stand-alone AIRS radiative transfer algorithm (Strow *et al.* 2003) to compute brightness temperatures from background fields for AIRS. We use the radiative transfer algorithm of Rosenkrantz (2003) for AMSU-A channels. We then subtract the computed background brightness temperatures from the observations. As described in Joiner *et al.* (2004), we apply systematic error correction (tuning) to correct for biases in the observations and/or forward model.

We calculate two types of differences between brightness temperatures produced using the vertical and slanted atmospheric paths. The first difference is simply the difference between the calculated brightness temperatures using the background fields with the vertical (B_V) and slanted (B_S) atmospheres, denoted ΔB. The second difference, $\Delta|O - B| = |O - B_V| - |O - B_S|$, is designed to assess whether the use of the slanted atmospheric path improves upon the use of the vertical path. A positive (negative) value of $\Delta|O - B|$ denotes an improvement (degradation) of the computed brightness temperature by using the slanted path compared with that using the vertical path as measured by the distance from the observation.

6. Results obtained with AIRS and AMSU-A data

Figure 3 shows the globally averaged channel standard deviations of the brightness temperature differences between calculations using vertical and slanted atmospheres (ΔB). For reference, we also show the detector noise values in terms of noise-equivalent temperature (NEΔT). For AIRS channels, we took the reported NEΔT values at a reference temperature of 250 K (S. Y. Lee, personal communication) and computed a value of NEΔT at each cloud-free observed brightness temperature. Average values $\pm 1\sigma$ of NEΔT for each channel are shown.

For most channels, the standard deviations of ΔB are well below the detector noise. However, they are comparable to the noise for some channels in the 6.7 μm water vapour band. Differences should approach zero as the peaks of the channel weighting functions move towards the surface. Non-zero differences appear for window channels because our slanted calculations reproduce the effect of mountains blocking the emission; we recalculate the location of the off-nadir pixel at the intersection of the line-of-sight with the projected footprint on the earth's surface with the GMAO model terrain.

Figure 4 is similar to Fig. 3, but shows the maximum brightness temperature differences of ΔB for each channel. Few profiles produce brightness temperature differences of these magnitudes. For example, approximately 0.0005% (0.003%) of the observations had brightness temperature differences greater than 2(1) K. However, it can be seen that these differences are comparable to or significantly greater than the instrument noise for most AMSU-A channels and many AIRS channels, especially those in the 6.7 μm H_2O band and in the most absorbing CO_2 channels in both the 15 μm and 4 μm bands. The latter channels have tails in their weighting functions that reach into the mesosphere. Note that AMSU channels 3–5 are not shown because the maximum values are quite large. This is due to a mountain blocking the path to the surface near a coastline. In this case, the mountain significantly changed the surface emissivity of the pixel whose footprint location was originally over ocean.

The locations of the profiles that produce large differences vary with channel owing to changes in the peaks of the weighting functions and the particular absorber affecting a given channel. Figure 5 shows locations where ΔB is significant for a sample of channels. Profiles that produce large differences in temperature-sensitive AMSU channels and AIRS channels in the 15 μm and 4 μm bands are concentrated in the northern hemisphere at middle to high latitudes where there are substantial temperature gradients. Figure 5 shows that the locations for the high-peaking AIRS channel at 667.9 cm^{-1} (peak of the weighting

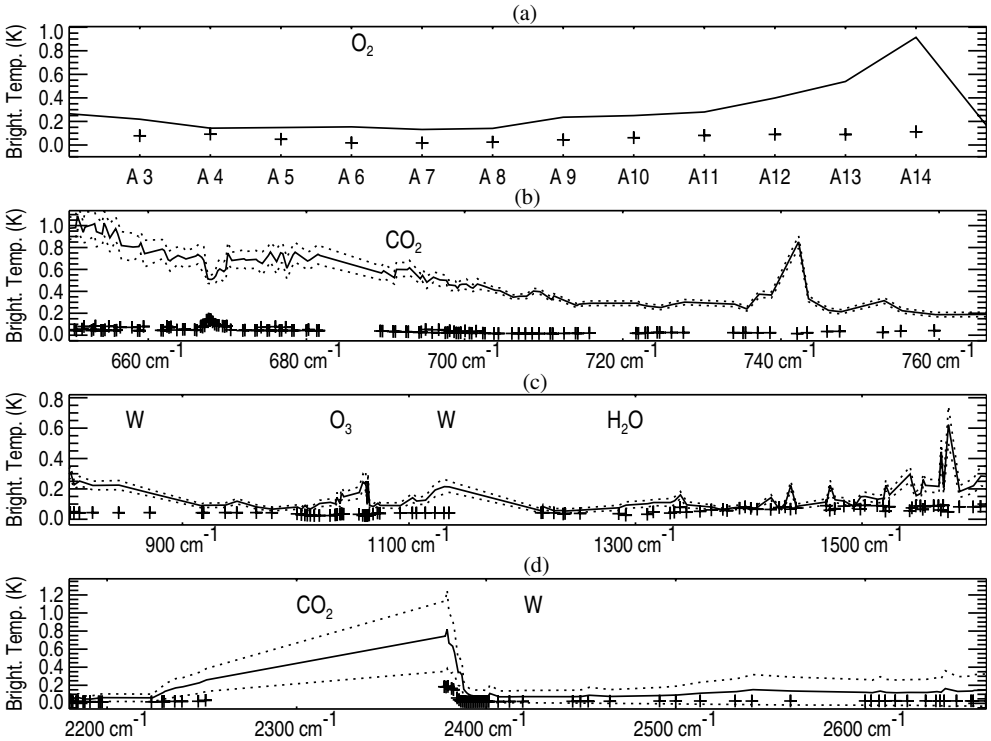

Figure 3. Standard deviations of ΔB (+) and average $\pm 1\sigma$ (solid and dotted lines) of the instrument noise (NEΔT) for (a) AMSU-A channels and (b)–(d) AIRS channels. Major absorption bands are indicated above the curves with window regions denoted by 'W'. (See text for definitions.)

function ~2 hPa and tail in the mesosphere) are at lower latitudes than for the lower-peaking AMSU channel 10 (weighting function peak ~50 hPa). Profiles that produce the largest differences in upper tropospheric humidity channels are scattered mainly throughout the tropics. Locations that produce the largest differences in the ozone-sensitive channels occur in the northern hemisphere where there are large gradients in ozone as well as temperature. The surface-sensitive channels have the largest differences in Antarctica and a few other locations where there are large gradients in elevation.

Figure 6 shows the global mean value of $\Delta|O - B|$ for each channel. Degradations (negative values) can be seen in the very high-peaking temperature sounding (CO_2) channels in the 15 μm and 4 μm bands. These channels are sensitive to temperatures at altitudes above the highest analysis level (0.4 hPa). Above this level, the atmospheric fields are those given by the GMAO forecast forced from below by observations primarily from the NOAA operational AMSU-A instruments. (Note that Aqua AMSU-A data were not assimilated in the fields used here.) The negative values for these channels suggest that the temperature gradients at these altitudes in the background field may contain errors.

Similarly, we observe negative values of the mean $\Delta|O - B|$ for the highest-peaking water vapour channels in the 6.7 μm band. The water vapour data in the upper troposphere used in the NCEP analysis come primarily from HIRS channel 12. The weighting function of this channel peaks below the most absorbing AIRS water vapour channels. Therefore, the data going into the analysis may not be good enough to provide information on the gradients in water vapour occurring in the upper troposphere at altitudes where the highly absorbing AIRS channel weighting functions peak.

In contrast, we see improvements (positive values) in the lower-peaking tropospheric temperature-sensitive channels in both the 15 μm and 4 μm bands, with the greatest improvements occurring for the higher peaking of these channels. As the weighting functions move towards the surface, the values of ΔB become small because dx as shown in Fig. 1 goes to zero with dz.

We see improvement in the ozone-sensitive channels. The ozone analysis uses observations from SBUV that are very accurate in the middle to upper stratosphere. It appears that the ozone analysis is

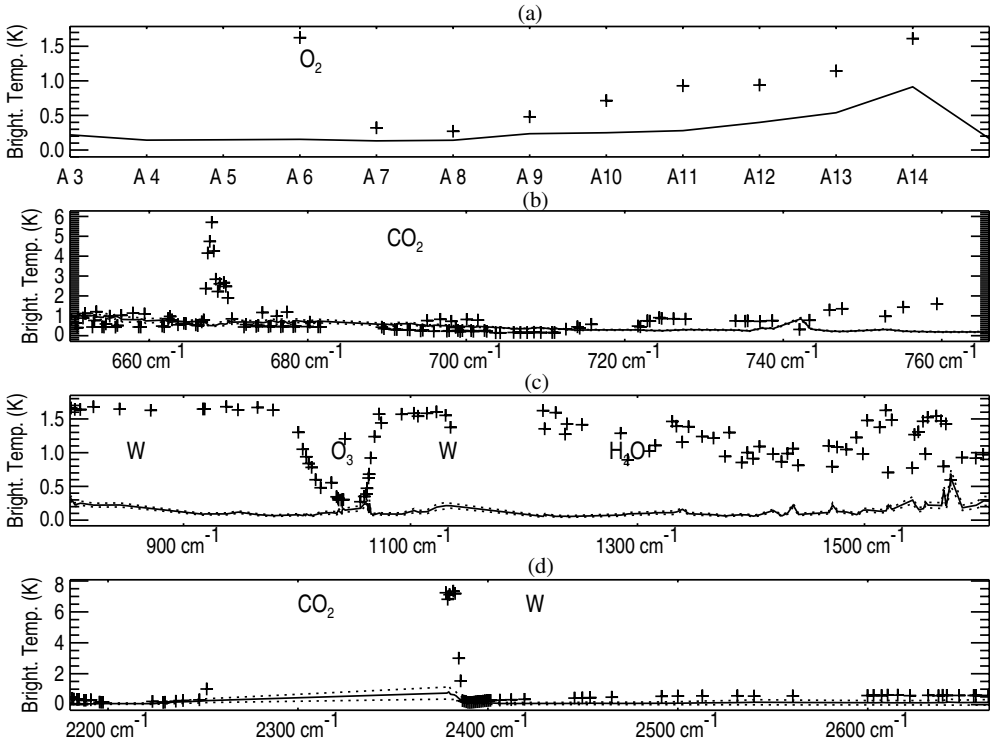

Figure 4. As Fig. 3, but showing maximum brightness temperature differences (+). Average $\pm 1\sigma$ values of NEΔT are replotted (solid and dotted lines) on this scale.

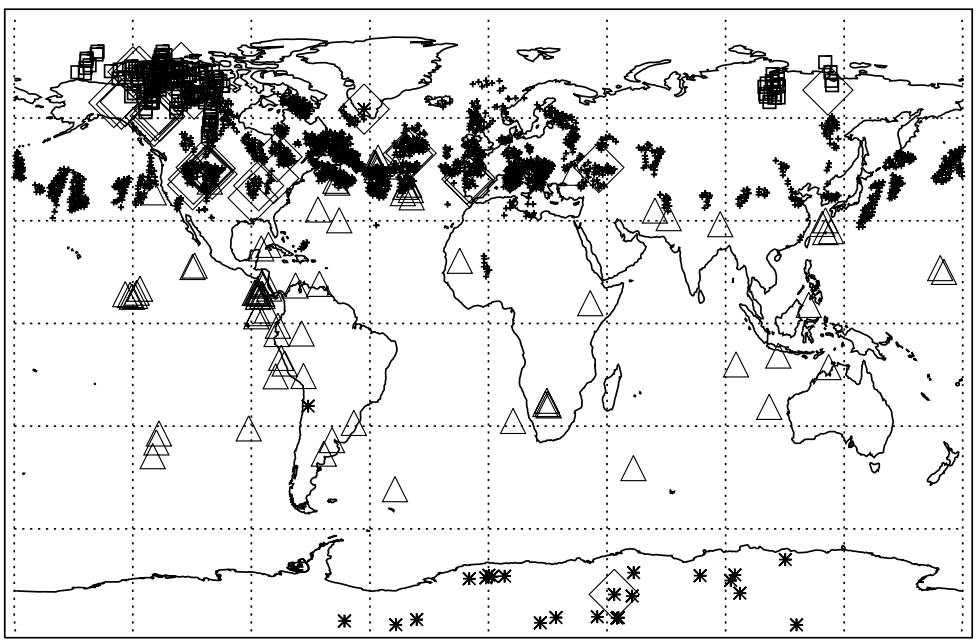

Figure 5. Locations of $\Delta B > x$ for AMSU 10 (middle stratosphere), $x = 0.5$ K (□); AIRS 667.9 cm^{-1} (upper stratosphere), $x = 0.5$ K (+); AIRS 1551.6 cm^{-1} (upper tropospheric H_2O), $x = 0.5$ K (△); AIRS 1039.9 cm^{-1} (O_3), $x = 0.2$ K (◇); AIRS 871.1 cm^{-1} (surface), $x = 0.2$ K (∗).

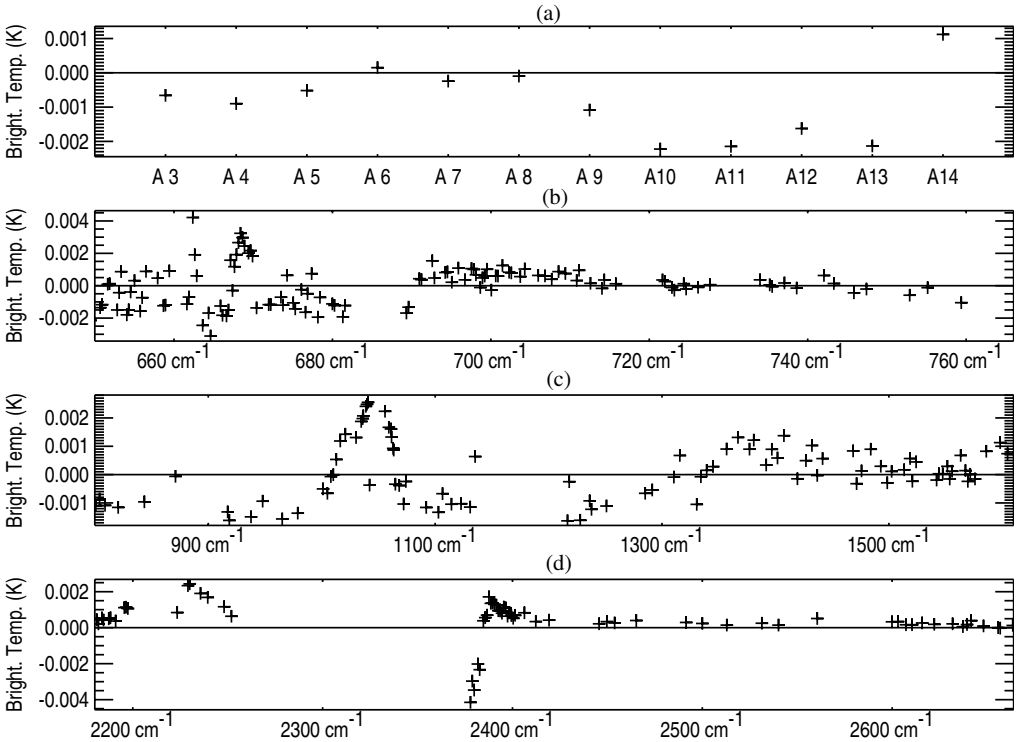

Figure 6. As Fig. 3, but showing mean values of $\Delta|O - B|$ (+).

providing accurate gradients in ozone that lead to improvements when the slanted atmospheric path is used to compute brightness temperatures.

Figure 7 shows the distributions of $\Delta|O - B|$ for a few representative channels. The histograms indicate that the mean improvement or degradation for a channel is primarily influenced by data in the wings of the distributions. For some channels there are improvements (degradations) near the centre of the distributions where the gradient effects are small, while the overall mean result was in the opposite direction due to degradations (improvements) in the wings of the distribution where the gradient effects were larger. For example, the stratospheric-peaking channels AMSU 10 and AIRS 666.9 cm^{-1} show improvement near the centre of the distribution, but an overall negative mean result. In contrast, the AIRS water-vapour-sensitive channel with frequency 1468.5 cm^{-1} shows a slight degradation near the centre, but an overall positive mean. Note that the differences in the total number of observations for the channels shown result from differences in detected cloud contamination.

7. Applications to Geostationary Earth Orbit (GEO)

Although the current study focuses on sounders in polar orbit, the effects of horizontal gradients should be considered for sounders on GEO platforms as well (see geometry in Fig. 8). Figure 9 shows that for latitudes as low as 43° (the latitude of Syracuse, New York or Marseilles, France), the satellite zenith angle will be greater than 50° for a GEO sounder.

From section 6, we have seen that for AIRS and AMSU the effects of horizontal gradients can be significant at these latitudes (and corresponding satellite zenith angles).

Furthermore, gradient effects may be even more important for future high-spectral-resolution infrared sounders with high horizontal resolution. The proposed Geosynchronous Imaging Fourier Transform Spectrometer (Smith *et al.* 2004) has a horizontal resolution of 4 km. Figures 2 and 9 show that, for example, for emission originating from $\mathrm{d}z = 10$ km above the surface at 43° latitude, there is 12 km distance $\mathrm{d}x$ between the vertical and the slanted lines-of-sight. Therefore, using the correct emission paths could help to extend the accuracy and range of useful latitudes for such GEO sounders.

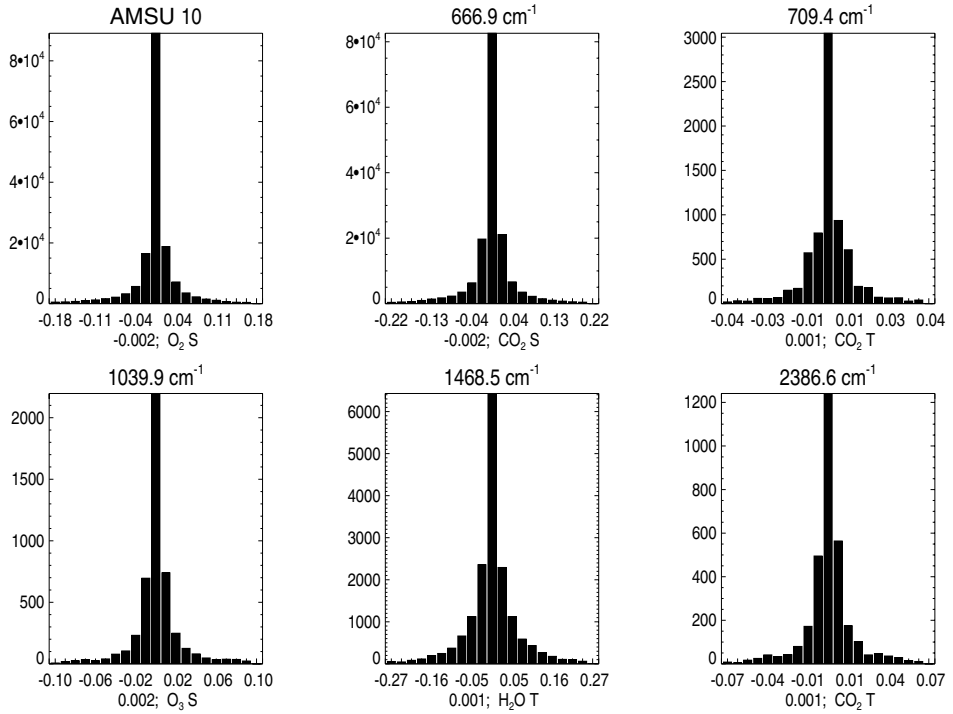

Figure 7. Histograms of $\Delta|O - B|$ for selected channels (x-axis units are K). The mean value (K) is indicated at the bottom, with the primary absorber and region of absorption, T (S) for troposphere (stratosphere).

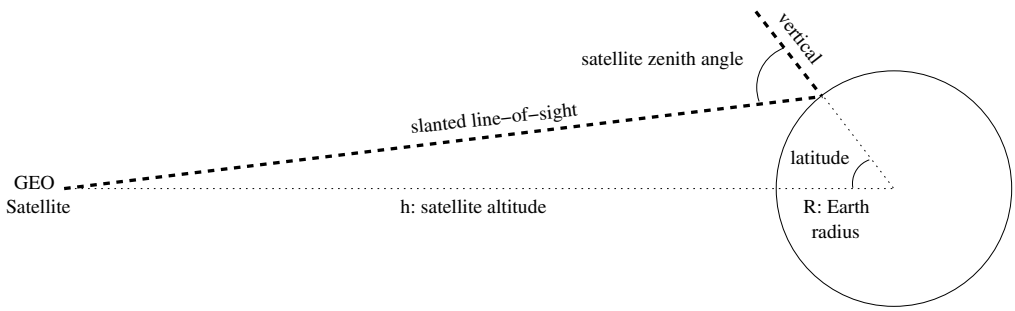

Figure 8. Geometry for a sounder on a GEO platform.

8. Conclusions and future work

We have shown that the overall effects of horizontal gradients are relatively small for most AIRS and AMSU-A channels. However, there are a few cases where the effects can be greater than the instrument noise for channels whose weighting functions peak in the upper troposphere and above. The effects are relatively small for the channels that are the most sensitive for numerical weather prediction (middle to lower tropospheric temperature and humidity channels), but are larger for stratospheric temperature channels and the most absorbing AIRS humidity channels in the upper troposphere. Our results suggest that the global analyses used here are capturing gradients well for tropospheric temperature and stratospheric ozone, but less well for upper-tropospheric humidity and upper-stratospheric and mesospheric temperature where the data used in those analyses are limited. Note that the results obtained here are dependent upon the analyses used and should be repeated in the future when higher-resolution or higher-quality analyses are available.

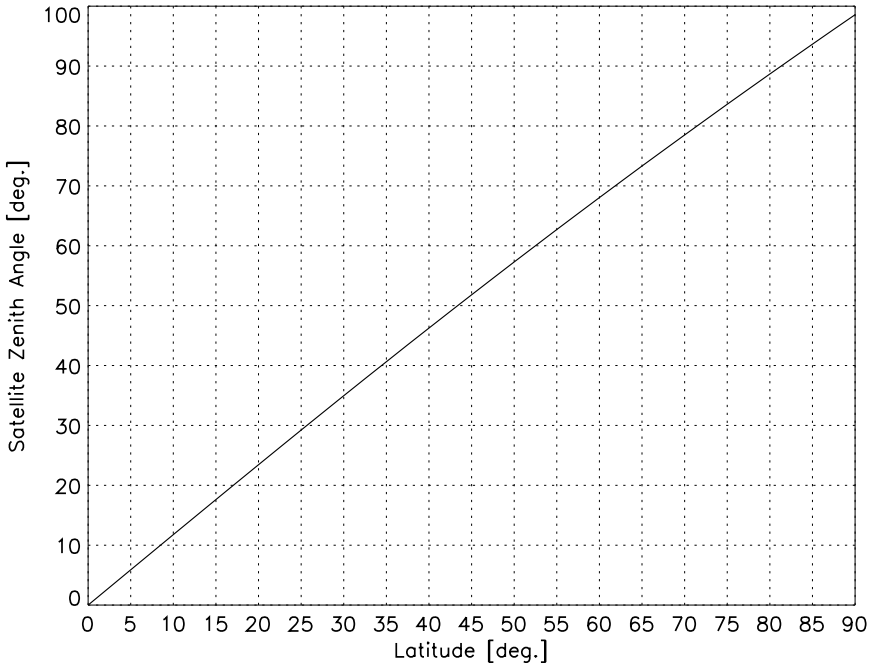

Figure 9. Satellite zenith angle as a function of latitude for four altitudes 0, 10, 20, and 30 km. These appear as a single line.

The methodology developed here also has applications for other types of nadir-viewing instruments. For example, nadir-viewing ultraviolet and visible radiometers, such as the Ozone Monitoring Instrument (OMI) flying on NASA's EOS Aura, are sensitive to the scattered path of solar photons. Horizontal gradient effects may be particularly important at high solar zenith angles. These conditions typically occur at high latitudes for instruments on polar-orbiting satellites where large gradients in ozone can occur at the edges of the polar vortex. The results shown for GEO sounders would also apply for future UV instruments in that orbit due to the combination of high solar and satellite zenith angles. We plan to do a similar study for OMI and other solar backscatter UV instruments. The results may have implications for the validation of the total column ozone produced with such instruments including inter-instrument comparisons.

Acknowledgements

The authors thank the AIRS science team, especially M. Goldberg and W. Wolf, for providing the AIRS and AMSU-A data and L. Strow and P. Rosenkrantz for providing the radiative transfer codes. We also thank two anonymous reviewers and Jonathan Taylor for valuable comments that improved the manuscript. This work was supported by a grant from NASA through the NOAA/NASA/DoD Joint Center for Satellite Data Assimilation.

References

Aumann, H. H., Chahine, M. T., Gautier, C., Goldberg, M. D., Kalnay, E., McMillin, L. M., Revercomb, H., Rosenkrantz, P. W., Smith, W. L., Staelin, D. H., Strow, L. L. and Susskind, J. 2003 AIRS/AMSU/HSB on the Aqua Mission: Design, science objectives, data products, and processing systems, *IEEE Trans. Geosci. Remote Sensing*, **41,** 253–264

Cohn, S. E., da Silva, A. M., Guo, J., Sienkiewicz, M. and Lamich, D. 1998 Assessing the effects of data selection with the DAO physical-space statistical analysis system, *Mon. Weather Rev.*, **126,** 2913–2926

Derber, J. and Wu, W.-S. 1998 The use of cloud-cleared radiances in the NCEP SSI analysis system. *Mon. Weather Rev.*, **126,** 2287–2299

Goldberg, M. D., Qu, Y., McMillin, L. M., Wolf, W., Zhou, L. and Divakarla, M. 2003 AIRS Near-real-time products and algorithms in support of operational numerical weather prediction. *IEEE Trans. Geosci. Remote Sensing*, **41,** 379–389

Joiner, J., Poli, P., Frank, D. and Liu, H. H. 2004 Detection of cloud-affected AIRS channels using an adjacent-pixel approach. *Q. J. R. Meteorol. Soc.*, **130,** 1469–1487

Kiehl, J. T., Hack, J. J., Bonan, G. B., Boville, B. A., Briegleb, B. P., Williamson, D. L. and Rasch, P. J. 1996 'Description of the NCAR Community Climate Model (CCM3)'. Technical Note TN-420+STR, NCAR, Boulder, USA

Lin, S.-J. 1997 A finite-volume integration method for computing pressure gradient forces in general vertical coordinates. *Q. J. R. Meteorol. Soc.*, **123,** 1749–1762

Poli, P. 2004 Effects of horizontal gradients on GPS radio occultation observation operators. II: A Fast Atmospheric Refractivity Gradient Operator (FARGO). *Q. J. R. Meteorol. Soc.*, **130,** 2807–2825

Poli, P. and Joiner, J. 2004 Effects of horizontal gradients on GPS radio occultation observation operators. I: Ray-tracing. *Q. J. R. Meteorol. Soc.*, **130,** 2787–2805

Rosenkrantz, P. W. 2003 Rapid radiative transfer model for AMSU/HSB channels. *IEEE Trans. Geosci. Remote Sensing*, **41,** 362–368

Smith, W. L, Revercomb, H. E., Bingham, G., Huang, H.-L., Zhou, D. K., Velden, C. S., Miller, J. B. and Emmitt, G. D. 2004 'GIFTS—Hyperspectral imaging and sounding from geostationary orbit'. Paper 14.6 in preprints for 20th Internat. Conf. on Interactive Information and Processing Systems (IIPS) for Meteorology, Oceanography, and Hydrology, Seattle, 11–15 January 2004. American Meteorol. Soc., Boston, USA

Stajner, I., Riishøjgaard, L. P. and Rood, R. B. 2001 The GEOS ozone data assimilation system: specification of error statistics. *Q. J. R. Meteorol. Soc.*, **127,** 1069–1094

Strow, L. L., Hannon, S. E., De Souza-Machado, S., Motteler, H. E. and Tobin, D. 2003 An overview of the AIRS radiative transfer model. *IEEE Trans. Geosci. Remote Sensing*, **41,** 303–313